JOC The Journal of Organic Chemistry

Article

pubs.acs.org/joc

In Silico Design of Halogen-Bonding-Based Organocatalyst for Diels–Alder Reaction, Claisen Rearrangement, and Cope-Type Hydroamination

Choon Wee Kee and Ming Wah Wong*

Department of Chemistry, National University of Singapore, 3 Science Drive 3, Singapore, Singapore 117543

Supporting Information

ABSTRACT: Using DFT calculations, we investigated the use of halogen bonding (XB) interactions to accelerate and control organic reactions, namely Diels–Alder reaction, Claisen rearrangement, and Cope-type hydroamination. Our designed triarylbenzene tripodal organocatalyst is characterized by three halogen bond donors, perfluoro-iodophenyl groups. The calculated transition states unravel multiple halogen bonds between the iodine atoms and various types of halogen bond acceptors (lone pair, π and σ bonds). These cooperative noncovalent interactions provide efficient binding between the catalyst and substrate (~15 kcal/mol binding energy) and are the key factors for transition-state stabilization and molecular recognition. On the basis of our DFT calculations and calculated turnover frequencies, the XB-catalyzed reactions are found to be competitive with the corresponding hydrogen bonding catalysis reported in literature.

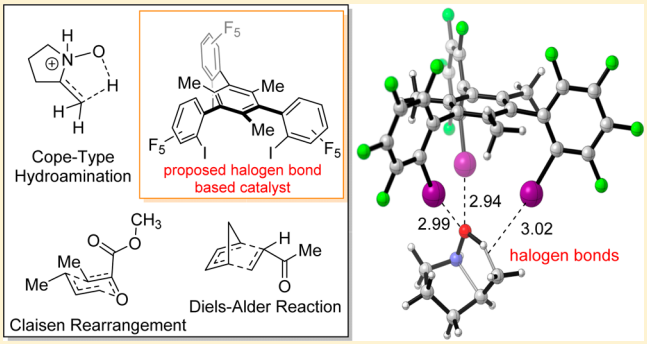

1. INTRODUCTION

Halogen bonding (XB) is a noncovalent interaction between a halogen atom (X) acting as a Lewis acid and an electron donor acting as a Lewis base.[1] The high directionality and strength of halogen bond make it one of the key noncovalent interactions in crystal engineering and supramolecular chemistry.[2] XB has also been recognized as an important noncovalent interaction in biology.[3] Within the past years, there is an increasing amount of research which aims to harness XB in organocatalysis.[4] The group of Huber is particularly active in this aspect.[4b,d,e,5] We have also disclosed an example where XB is used as a key noncovalent interaction in enantioselective reaction through a combination of experimental results and theoretical calculations.[6] The parallel between the hydrogen bond and halogen bond (X-bond) in terms of high directionality and strength has been recognized.[7] Given the ubiquitous applications of hydrogen bond as key interactions in organocatalysis,[8] the potential of halogen bond in organocatalysis is evident.

In this work, we have explored and demonstrated the feasibility of halogen bond catalysis in a Diels–Alder reaction, Claisen rearrangement, and Cope-type hydroamination, through an *in silico* designed XB-based neutral organocatalyst. These reactions are known to be accelerated by hydrogen-bonding-based catalysts. Our *in silico* catalyst design is inspired by a tripodal hydrogen bond anion receptor reported by Wang, Kass and co-workers.[9] We replaced the three hydroxyl functional groups of the triarylbenzene with halogens (Figure 1) and studied the catalytic cycle of typical Diels–Alder, Claisen, and Cope-type hydroamination reactions via DFT calculations.

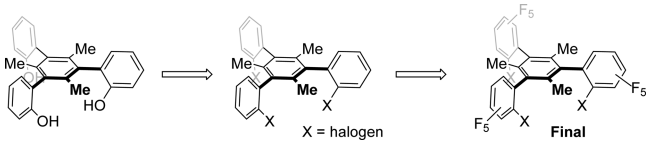

Figure 1. Design of halogen-bonding-based tripodal organocatalyst.

Recently, Huber, Waldvogel and co-workers have demonstrated that a related molecule could bind acetone in a tridentate mode.[10] We envisaged that such a tridentate binding model could activate an α,β-unsaturated carbonyl as a dienophile, thereby accelerating a Diels–Alder reaction. For Claisen rearrangement, the increase of partial negative charge on the ether oxygen from the substrate or pretransition state (pre-TS) complex to the transition state (TS) is the basis of hydrogen bond-catalyzed Claisen rearrangement (Figure 2).[11] As the strength of XB stabilization is also dependent on the negative charge present on the X-bond acceptor,[12] we hypothesized that XB could also play a critical role in accelerating Claisen rearrangement. Based on the same principle of increasing partial charge in the transition state (Figure 2) as basis of accelerating a hydrogen-/halogen-

Received: May 16, 2016
Published: August 3, 2016

DOI: 10.1021/acs.joc.6b01147
J. Org. Chem. 2016, 81, 7459–7470

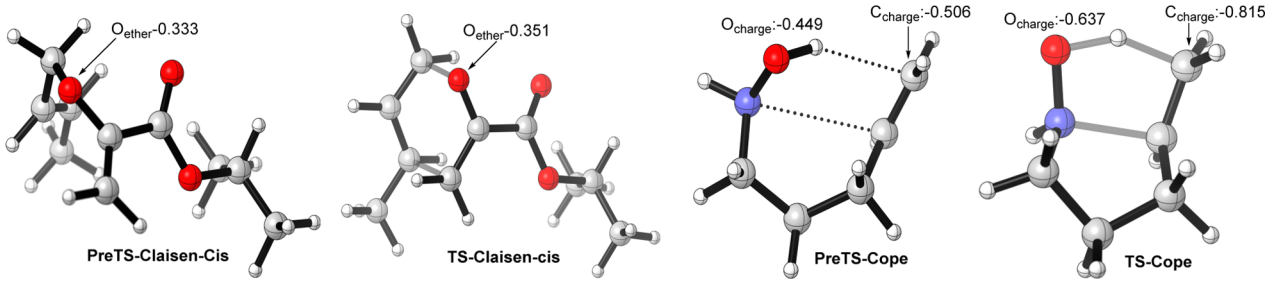

Figure 2. Comparison of atomic charges (MK-ESP) between the pre-TS and TS for uncatalyzed Claisen rearrangement and Cope-type hydroamination.

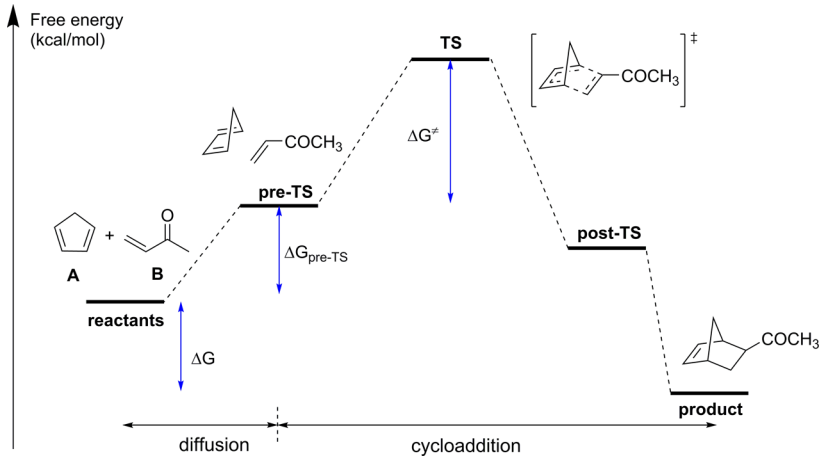

Figure 3. Definition of ΔG, $\Delta G_{\text{pre-TS}}$, and $\Delta G^{\ddagger}$ using Diels–Alder reaction as an illustration.

bonding-based reaction, Cope-type hydroamination[13] presents also an attractive opportunity to further exploit XB in organocatalysis. Acceleration of Cope-type hydroamination by a protic solvent has been observed by Beauchemin and co-workers.[14] Jacobsen and co-workers postulated that the hydrogen bonding interaction of the thiourea catalyst with the substrate is able to accelerate this reaction.[15]

2. COMPUTATIONAL METHODS

The M06-2X[16] functional was employed in this study as this empirical functional is better suited than the normal hybrid DFT methods (e.g., B3LYP) for handling noncovalent interactions (include halogen bond).[16a,17,18] Two basis sets, SMALL and LARGE, were used for geometry optimizations and single-point energy calculations, respectively. The SMALL basis set comprises the standard 6-31G(d) basis set for all atoms except bromine and iodine, while the BIG basis set comprises a larger 6-311+G(d,p) basis set for all atoms except bromine and iodine. In both the SMALL and BIG basis set, the aug-cc-pVTZ basis set together with the SDB pseudopotential was used for bromine and iodine,[19] obtained from basis set exchange.[20] For the single-point calculations with a larger basis set, a larger integration (via int = ultrafine) grid was employed. The solvent effect is modeled by the SMD implicit solvation model.[21] Unless otherwise noted, relative energies (ΔH and ΔG) reported in the text correspond to the M06-2X/BIG//M06-2X/SMALL level of theory at 298.15 K. Density functional theory (DFT) calculations were performed with the Gaussian 09 suite of programs,[22] while benchmark CCSD(T)-F12[23] calculations were carried out with the MOLPRO 2015 program.[24]

Visualization of noncovalent interactions in the transition state was carried out using the NCI plot.[25] The NCI isosurfaces were calculated with NCIplot[26] and visualized with Visual Molecular Dynamics (VMD) software.[27] In NCI plots, green represents weakly attractive while blue denotes strongly attractive. Images are rendered from POVRAY with script generated from CYLview.[28]

Translating Calculated Barrier to Rate Constants. Investigating a reaction pathway by locating key stationary points on the relevant potential energy surface provides us with the energetic landscape. However, a connection between this energy landscape and the experimental observable, in the form of rate constant, is required in order to correlate the computational result with the experimental finding. For a simple unimolecular reaction, the transition state theory readily provides this connection by transforming the activation barrier into a rate constant. For a bimolecular reaction, as in the case of the Diels–Alder reaction, the reaction can be described as two consecutive molecular processes: diffusion of reactants to form the reactive intermediate/pre-TS complex and the actual cycloaddition (Figure 3).

The free energy of activation ($\Delta G^{\ddagger}$) of the cycloaddition reaction can be obtained as the difference between the free energies of the TS and pre-TS complex, with the basic assumption that the diffusion of reactants is a barrier-free process. For the uncatalyzed reactions examined in this paper, we adopted a pre-equilibrium kinetic model where we assume that equilibrium between the pre-TS and the free reactants (A and B) can be attained (eq 1).

$$\frac{\mathrm{d[product]}}{\mathrm{d}t} = kK_{\text{eq}}[A][B], \quad k = \text{rate constant}, \tag{1}$$

K_{eq} = equilibrium constant

Thus, the equilibrium constant is given by eq 2.

$$K_{\text{eq}} = e^{-(G_{\text{preTS}} - G_{\text{A}} - G_{\text{B}})/RT} = e^{-\Delta G/RT} \tag{2}$$

The rate constant is obtained from the conventional transition state theory (eq 3).

$$k = \frac{k_{\text{B}}T}{h} e^{-(G_{\text{TS}} - G_{\text{preTS}})/RT} = e^{-\Delta G^{\neq}/RT} \tag{3}$$

The pre-equilibrium rate constant is then given by eq 4.

DOI: 10.1021/acs.joc.6b01147
J. Org. Chem. 2016, 81, 7459–7470

$$kK_{eq} = \frac{k_B T}{h} e^{-(\Delta G^{\neq} + \Delta G)/RT} = \frac{k_B T}{h} e^{-(G_{TS} - G_A - G_B)/RT} \quad (4)$$

Therefore, the effective activation barrier is the difference between the free energies of the TS (G_{TS}) and the free reactant ($G_A + G_B$). This definition is used in the subsequent computational investigation. A pictorial representation of ΔG, $\Delta G_{pre\text{-}TS}$, and $\Delta G^{\ddagger}$ is given in Figure 3.

Defining the activation barrier as the difference between the free energies of TS and the free reactants (i.e., A and B) will generally overestimate the translational and rotational entropy loss. A correction of −2.6 kcal/mol for a reaction transforming two molecules into one has been proposed by Li and Zhou.[29] However, we have not applied any correction, as it does not change our conclusion.

Energetic Span Model. In the case of a catalytic reaction, we employed the energetic span model of Shaik and Kozsch.[30] This model captures the influence of intermediates and transition states in the calculation of turnover frequency (TOF). In the case where the TOF is determined by only one intermediate and one transition state, these are defined as the turnover determining intermediate (TDI) or transition state (TDTS). Otherwise, the influence of the intermediate and transition on TOF is measured by their degree of TOF control.

TOF is independent of catalyst concentration, and its relationship to the experimentally observed reaction rate is given by eq 5.

$$\text{TOF} = \frac{\text{rate}}{[\text{catalyst}]} \quad (5)$$

Experimentally, the rate is measured under the saturation kinetic condition, i.e. the region where substrate concentration does not affect the reaction.

TOF measures the turnover frequency of a reaction catalyzed by a particular catalyst. It can be converted to the reaction rate by multiplying with the initial catalyst concentration (TOF × [catalyst], for example a TOF of 10 h^{-1} and catalyst concentration of 0.01 mM will produce the product at a rate of 0.1 mM/h). In this study, TOF calculations were performed with the AutoTOF program.[32] For the uncatalyzed reactions examined in this paper, we used the pre-equilibrium kinetic model to gauge the concentration independent rate constants under the pseudo-zero-order condition. This is to allow for comparison with TOF calculated by AutoTOF for the catalytic reactions.

3. RESULTS AND DISCUSSION

3.1. Diels−Alder Reaction. Experimentally, XB catalysis in Diels−Alder reaction has been shown to be feasible by the groups of Huber[4d] and Takeda,[4f] and in both studies, the authors reported the use of cationic X-bond donor (XBD) as organocatalysts. Neutral bidentate XBDs are reported as organocatalysts for transfer hydrogenation of quinoline by the group of Bolm[4a] and the nucleophilic displacement reaction by the group of Huber.[4b] However, to the best of our knowledge, no neutral XBD has been reported for the Diels−Alder reaction. The use of neutral XBD has the advantage over ionic XBD in that a potential Lewis basic counteranion is absent. Huber and co-workers have demonstrated that a Lewis basic counteranion such as triflate could potentially coordinate to the XB-based catalysts and quench its catalytic activity.[4d]

Design of Catalyst. It is instructive to examine initially the effect of multiple halogen bonds on the activation barrier. To this end, various numbers of iodobenzene were considered as XB catalysts for the Diels−Alder reaction of cyclopentadiene with buten-2-one. The halogen bond donor, iodobenzene, serves as a Lewis acid catalyst. The potential of the multidentate X-bond in stabilizing the transition state of the Diels−Alder reaction is evident from the calculated activation enthalpies ($\Delta H^{\ddagger}$) in Table 1. Compared to the uncatalyzed reaction, the formation of the X-bond between iodobenzene and buten-2-one lowers the $\Delta H^{\ddagger}$ by 4.3 kcal/mol. Inclusion of a second molecule of iodobenzene further reduces the $\Delta H^{\ddagger}$. With three iodobenzenes, the $\Delta H^{\ddagger}$ is reduced to −4.4 kcal/mol. The negative barrier is due to the formation of a fairly stable halogen-bonded pre-TS complex. However, unfavorable entropy contribution outweighs the stabilization effect, and the activation free energy ($\Delta G^{\ddagger}$) increases by approximately 5 kcal/mol with each iodobenzene catalyst added (Table 1). Halogen bonds, with an I···O distance of ∼3.0 Å, are observed in all transition states (Figure 4). In the case of **PhI-3**, the third iodine atom interacts with C═C π bond of buten-2-one, which serves as an X-bond acceptor (Figure 4).

Table 1. Calculated Activation Barriers (in kcal/mol) for Uncatalyzed and XB-Catalyzed Diels−Alder Reactions[a]

catalyst	$\Delta H^{\ddagger}$	$\Delta G^{\ddagger}$
nil	10.0	23.8
PhI-1	5.7	28.2
PhI-2	1.4	33.2
PhI-3	−4.4	38.7
CAT-3-PhI	−0.5	26.5
CAT-3-perFPhI	−5.2	21.3

[a]Only *endo* product is considered.

One plausible solution to reduce the Gibbs free energy of activation is to pay for the entropy cost in the synthesis step, by building a molecule with three iodobenzenes in a suitable geometrical arrangement to reproduce the three key XB interactions in **PhI-3**. Based on the triarylbenzene core structure of Wang, Kass and co-workers,[9] a tripodal catalyst **CAT-3-PhI** (Figure 1) was tested *in silico*. The calculated $\Delta H^{\ddagger}$ is higher than that in **PhI-3**, but the $\Delta G^{\ddagger}$ is reduced significantly by about 12 kcal/mol. However, the predicted $\Delta G^{\ddagger}$ of **CAT-3-PhI** is higher than in the case of the uncatalyzed reaction (Table 1).

Further improvement to **CAT-3-PhI** could be achieved by exploiting the well documented fact that, for a given structure, an electron-withdrawing group on the halogen bond donor increases the strength of the X-bond.[31] With this in mind, a modified catalyst **CAT-3-perFPhI**, with three perfluoro-iodophenyl groups (Figure 1), was tested. Indeed, $\Delta H^{\ddagger}$ decreases to −5.2 kcal/mol and a corresponding decrease in $\Delta G^{\ddagger}$ to 21.3 kcal/mol occurred. Compared to the uncatalyzed Diels−Alder reaction, the $\Delta G^{\ddagger}$ of the **CAT-3-perFPhI**-catalyzed reaction is lowered by 2 kcal/mol. Thus, we expect our designed neutral XB-based catalyst to accelerate the Diels−Alder reaction between cyclopentadiene and buten-2-one.

Analysis of Noncovalent Interactions in Diels−Alder TS. The most stable TS for the **CAT-3-perFPhI**-catalyzed Diels−Alder reaction is shown in Figure 4. The noncovalent interactions (NCI) index developed by Yang and co-workers enables the visualization of noncovalent interaction.[25] The result of NCI analysis transforms noncovalent interaction from the reduced density gradient into the surface, in which color is representative of the nature (repulsive or attractive) and strength of the NCI. Two halogen bonds between the lone pairs of carbonyl and iodines are evident from the NCI isosurface (Figure 5).

The bidentate halogen bond lengths are similar (2.98 and 3.00 Å). One additional X-bond between iodine and the π bond of C═C is also observed. In addition to forming an X-bond with 2-butenone, the lone pairs of the iodine also form multiple C−H···I hydrogen bonds (refer to Figure S3 and Supporting Information (SI) for further discussion). These multiple

DOI: 10.1021/acs.joc.6b01147
J. Org. Chem. 2016, 81, 7459−7470

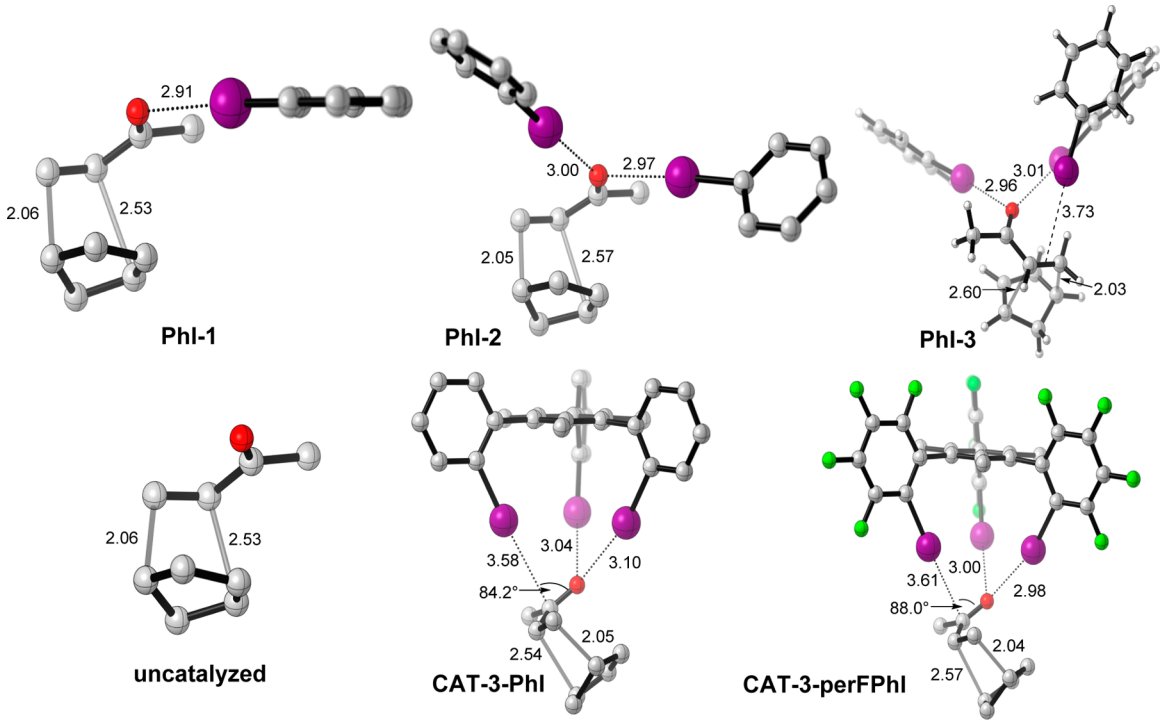

Figure 4. Optimized transition state structures for various catalyzed Diels–Alder reactions.

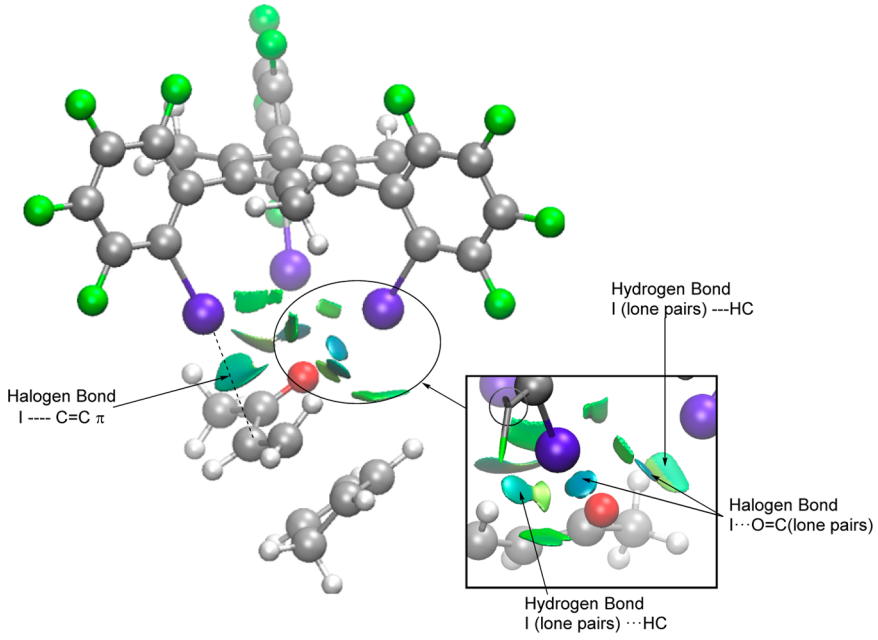

Figure 5. NCI isosurface between the substrate and catalyst for the transition state of **CAT-3-perFPhI**-catalyzed Diels–Alder reaction. Key intermolecular distances are given in Figure 6. Interaction strength increases from green to blue.

noncovalent interactions act together to stabilize the TS, which is readily manifested in the negative $\Delta H^{\ddagger}$ of the **CAT-3-perFPhI**-catalyzed reaction (Table 1).

We have adopted a fragment-based approach to estimate the noncovalent stabilization between each perfluoro-iodophenyl group of **CAT-3-perFPhI** and the substrates. The stabilization energy, $\Delta E_{int} = E_{TS} - (E_{\textbf{CAT-3-perFPhI}} + E_{substrate})$, is computed by partitioning **CAT-3-perFPhI** to isolate the noncovalent interactions that are associated with each of the perfluoro-iodophenyl groups present in **CAT-3-perFPhI** (Figure 6). Using this approach, the X-bond between iodine and the C=C π bond provides 4.1 kcal/mol of stabilization (Figure 6a). For the X-bond involving the oxygen lone pair (i.e., **b** and **c** in Figure 6), the interactions energies are larger, 6.2 and 6.6 kcal/mol, respectively. The iodine involved in the X-bond labeled as **b** in Figure 6 is also involved in weaker interactions with the methyl C–H's in its vicinity, while the iodine involved in the X-bond labeled as **c** in Figure 6 is involved in a stronger sp^2 C–H···I hydrogen bond. This is manifested in the slightly larger interaction energy (ΔE_{int}) of about 0.4 kcal/mol. Our adopted

DOI: 10.1021/acs.joc.6b01147
J. Org. Chem. 2016, 81, 7459–7470

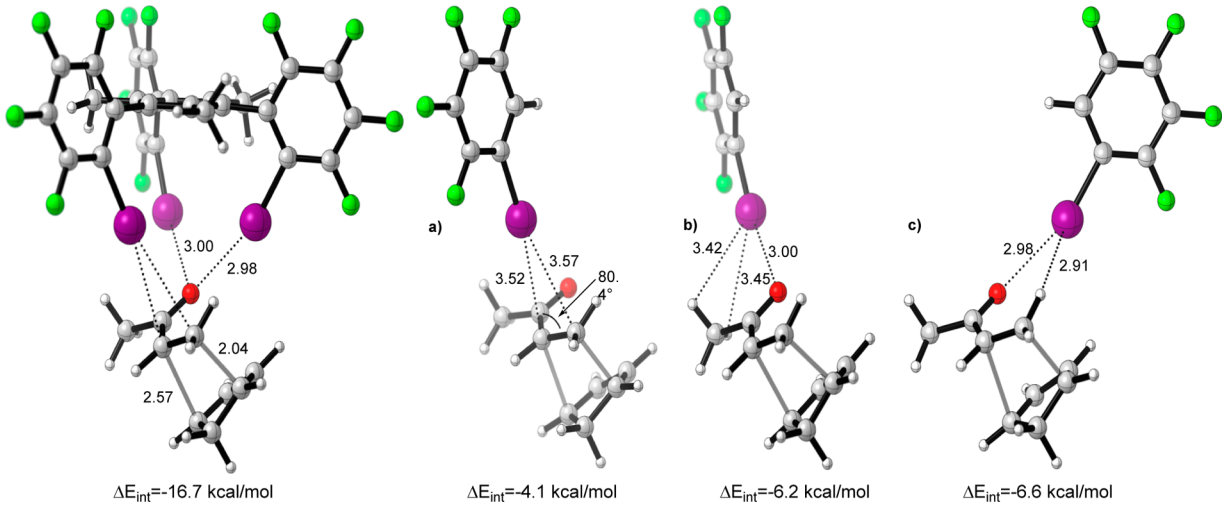

Figure 6. Fragment approach to estimate key noncovalent interactions in the transition state of **CAT-3-perFPhI**-catalyzed Diels–Alder reaction. The core of catalyst is replaced by a hydrogen with C–H bond length of 1.07 Å. Counterpoise correction is included in the calculated stabilization energy (ΔE_{int}).

fragment approach is validated by the fact that the total ΔE_{int} of the fragment (16.9 kcal/mol) is very close to the directly calculated interaction energy between **CAT-3-perFPhI** and substrates in the TS (16.7 kcal/mol).

Temperature Effect and TOF. From the definition of Gibbs free energy ($\Delta G^{\ddagger} = \Delta H^{\ddagger} - T\Delta S^{\ddagger}$), the unfavorable contribution of entropy to $\Delta G^{\ddagger}$ (mainly from the loss of translational entropy, if $S^{\ddagger} < 0$) could be minimized by reducing the reaction temperature. For the catalyzed reaction, the effect of reduction on the $T\Delta S$ term is larger than in the case of the uncatalyzed reaction, as the catalyzed reaction involves the assembly of three molecules but the uncatalyzed reaction only involves two molecules. The results in Table 2 are consistent with our argument. However, a reduction in barrier is insufficient to assess catalytic performance due to reasons that will be discussed in the following paragraph.

Table 2. Activation Barriers for Uncatalyzed and CAT-3-perFPhI-Catalyzed Diels–Alder Reaction, Rate Constant for Uncatalyzed Reaction and TOF for the Catalyzed Reaction at Various Temperatures

	uncatalyzed	catalyzed	uncatalyzed	catalyzed
temp (K)	$\Delta G^{\ddagger}$ (kcal/mol)		kK_{eq}[a]/M h^{-1}	TOF/h^{-1}
298.15	23.8	21.3	0.057	5.5
273.15	22.7	19.1	0.014	11
248.15	25.0	16.8	1.9×10^{-3}	28

[a]Pre-equilibrium kinetic model and pseudo-zero w.r.t. reactants condition is assumed.

A more realistic assessment of catalytic performance could be performed using the energetic span model of Shaik and Kozuch.[30,32] Lowering of the temperature has two main effects: (1) It reduces the amount of energy to overcome the kinetic barriers, and (2) it reduces unfavorable contribution from the entropy term in $\Delta G^{\ddagger}$. In the case of the uncatalyzed Diels–Alder rearrangement, the first effect dominates, and as a result, the rate constant is reduced despite the decrease in $\Delta G^{\ddagger}$ (Table 2). For the **CAT-3-perFPhI**-catalyzed reaction, the second effect dominates. Thus, the computed TOF increases with decreasing temperature; this reflects the lowering of $\Delta G^{\ddagger}$ which in this case is equal to the energetic span. At 248.15 K, the catalyzed reaction has a TOF of 28 h^{-1} while the uncatalyzed reaction is negligible (Table 2). This lends further support to our conclusion that our designed XB-based catalyst is applicable to the Diels–Alder reaction.

Endo/Exo Selectivity and Solvent Effect. Endo and exo selectivity is an important issue in Diels–Alder reaction. Our calculations indicate that, in the XB-catalyzed Diels–Alder reaction by **CAT-3-perFPhI**, the endo-product selectivity is increased significantly relative to the uncatalyzed reaction. The results are summarized in Table 3.

Table 3. Endo and Exo Selectivity for Uncatalyzed and CAT-3-perFPhI-Catalyzed Diels–Alder Reactions

	relative energy[a]	endo-C1	endo-C2	exo-C1	exo-C2
uncatalyzed	$\Delta\Delta H^{\ddagger}$	0.0	1.9	4.6	0.6
	$\Delta\Delta G^{\ddagger}$	0.0	2.4	4.5	0.3
catalyzed	$\Delta\Delta H^{\ddagger}$	0.0	2.5	5.6	1.3
	$\Delta\Delta G^{\ddagger}$	0.0	3.4	7.1	2.1

[a]In kcal/mol, temperature = 298.15 K. C1 and C2 define the relative orientation of the ketone group (see SI Figure S2 for details).

The effect of solvent on the activation barrier of both the uncatalyzed and **CAT-3-perFPhI**-catalyzed Diels–Alder reaction is modeled via the SMD implicit solvation model. We have chosen two common solvents, *n*-hexane and chloroform, for this purpose. The results are tabulated in Table 4. When the solvent effect is included, the barriers of both catalyzed and uncatalyzed reactions increase. Chloroform and *n*-hexane gave similar barriers for the uncatalyzed Diels–Alder reaction. For

Table 4. Effect of Solvent on Uncatalyzed and CAT-3-perFPhI-Catalyzed Diels–Alder Reactions at 248.15 K

	uncatalyzed	catalyzed	uncatalyzed	catalyzed
solvent	$\Delta G^{\ddagger}$ (kcal/mol)		kK_{eq}/M h^{-1}	TOF/h^{-1}
gas phase	21.6	16.8	1.9×10^{-3}	28.0
n-hexane	23.1	20.3	9.0×10^{-5}	2.5×10^{-2}
chloroform	23.1	22.1	8.5×10^{-5}	6.1×10^{-4}

DOI: 10.1021/acs.joc.6b01147
J. Org. Chem. 2016, 81, 7459–7470

Scheme 1. Model Claisen Rearrangement Reported by Hiersemann and Strassner et al. $\Delta G^{\ddagger}$ Is in kcal/mol

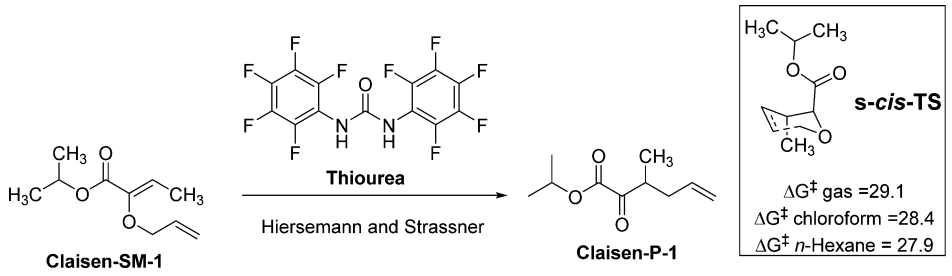

Table 5. Calculated Barriers (kcal/mol) of CAT-3-perFPhI-Catalyzed Claisen Rearrangement

barrier	CAT-3-perFPhI-s-*trans*-1	CAT-3-perFPhI-s-*trans*-2	CAT-3-perFPhI-s-*cis*-1	CAT-3-perFPhI-s-*cis*-2	uncatalyzed
$\Delta H^{\ddagger}$ (gas phase)	10.8	13.9	11.2	18.9	26.8[b]/27.1[c]
$\Delta H^{\ddagger}$ (*n*-hexane)[a]	12.0	15.3	12.4	19.5	26.1[b]/26.0[c]
$\Delta H^{\ddagger}$ (chloroform)[a]	13.1	16.2	13.6	19.3	25.7[b]/25.4[c]
$\Delta G^{\ddagger}$ (gas phase)	25.7	29.5	26.8	34.8	29.5[b]/29.1[c]
$\Delta G^{\ddagger}$ (*n*-hexane)[a]	27.3	31.2	28.5	35.9	29.2[b] /28.4[c]
$\Delta G^{\ddagger}$ (chloroform)[a]	28.5	32.3	29.8	35.9	28.9[b] /27.9[c]

[a]Solvent effect was examined with the SMD solvation model. [b]s-*trans* TS. [c]s-*cis* TS.

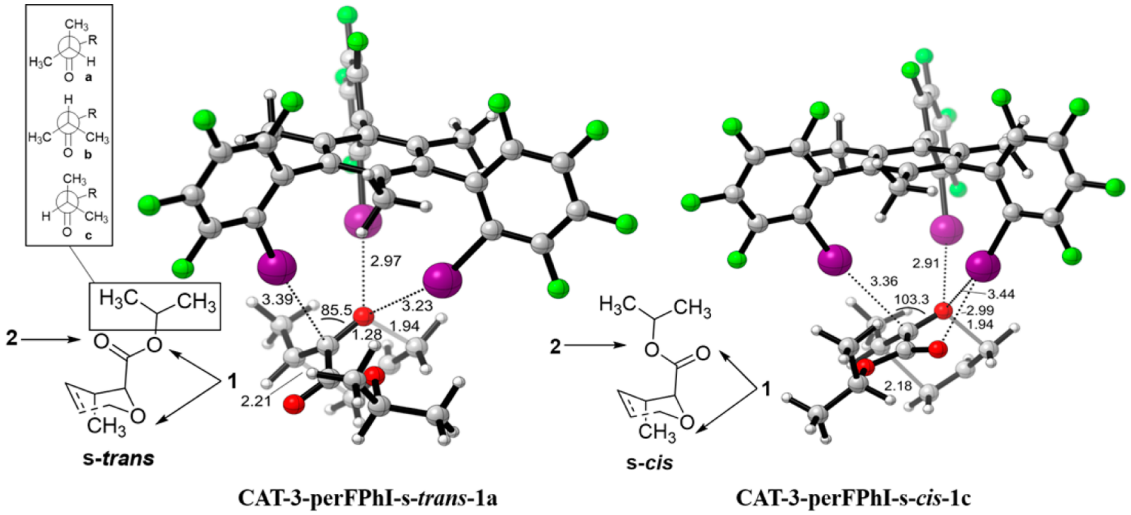

Figure 7. Conformational analysis for transition state of catalyzed Claisen rearrangement.

the catalyzed reaction, the barriers and the respective TOF increase with the inclusion of solvation effects. According to our calculations, chloroform reduces the TOF significantly.

3.2. Claisen Rearrangement. Claisen rearrangement is a powerful method to construct highly functionalized molecules.[33] The accelerating effect of protic solvents and Brønsted acids are well established in the literature. In particular, the work of Hiersemann, Strassner and co-workers reported that, in the presence of a stoichiometric amount of thiourea organocatalyst, thermal Claisen rearrangement is accelerated (Scheme 1).[34] Jacobsen and co-workers reported enantioselective Claisen rearrangement catalyzed by guanidinium salts.[35] These works have laid the foundation of hydrogen bonds as a key element in organocatalytic Claisen rearrangement.

Here, we studied the catalytic cycle of our designed XB-based catalyst **CAT-3-perFPhI** on the model Claisen rearrangement. The model substrate was chosen based on the work of Hiersemann and Strassner (Scheme 1). The effects of *n*-hexane and chloroform on the reaction barriers were modeled by the SMD solvation method. These solvents were chosen, as they were used experimentally by the groups mentioned in the preceding paragraph. The calculated barriers for thermal (uncatalyzed) Claisen rearrangement are given in Scheme 1. For both the gas- and solution-phase calculations, **s-*trans*-TS** and **s-*cis*-TS** gave almost identical barriers (see Table 5 and SI Table S1). The corresponding boat conformations (**s-*trans*-boat-TS** and **s-*cis*-boat-TS**) are highly unfavorable in terms of barrier, and therefore, they were not considered in subsequent calculations which involve **CAT-3-perFPhI** and **Thiourea** catalysts.

Conformational Analysis. Based on the s-*trans* and s-*cis* conformations of the uncatalyzed TS, two possible binding modes could be conceived, labeled as **1** and **2** in Figure 7. For the **CAT-3-perFPhI**-catalyzed rearrangement, conformation analysis leads to four possible TS conformations. For both s-*trans* and s-*cis* conformations, the most stable TS corresponds to the binding mode 1 (Figure 7). Additional conformations can be generated from rotation about the *i*-Pr group, and they are labeled based on the relative position of the methyl groups (Figure 7).

DOI: 10.1021/acs.joc.6b01147
J. Org. Chem. 2016, 81, 7459−7470

Table 6. Calculated Reaction Parameters of Uncatalyzed and Catalyzed Claisen Rearrangements Based on Conditions Reported by Hiersemann *et al.*[34]

	uncatalyzed		CAT-3-perFPhI	Thiourea	CAT-3-perFPhI	Thiourea
temp (K)	$\Delta G^{\ddagger}$ (kcal/mol)	kK_{eq}[a] (M h^{-1})	$\Delta G^{\ddagger}_{chloroform}$ (kcal/mol)		TOF (h^{-1})	
318.15	28.1	1.1×10^{-3}	29.5	30.7	1.2×10^{-4}	2.0×10^{-5}

[a]Pre-equilibrium approximation rate constant under pseudo zero order condition.

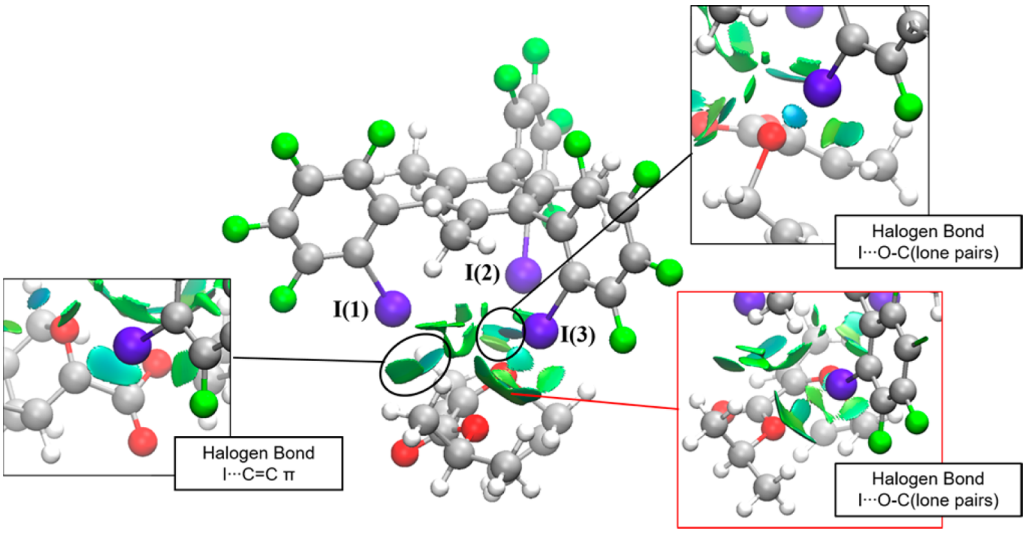

Figure 8. NCI isosurface of transition state **CAT-3-perFPhI-s-*trans*-1**.

The relevant calculated barriers for the **CAT-3-perFPhI**-catalyzed Claisen rearrangement are given in Table 5. The most stable TS, namely **CAT-3-perFPhI-s-*trans*-1**, have the lowest $\Delta H^{\ddagger}$ and $\Delta G^{\ddagger}$. These values are significantly less than the corresponding barriers in the gas-phase uncatalyzed reaction. Further analysis in terms of TOF will be given above (Table 6).

Analysis of Noncovalent Interaction in Claisen Rearrangement TS. The key noncovalent interactions in transition state **CAT-3-perFPhI-s-*trans*-1** is shown in Figure 8. All three iodine atoms, labeled as **1**−**3**, readily form halogen bonds with the substrate. By employing the same fragment-based approach adopted for the Diels−Alder reaction, the interaction energy due to each of the perfluoro-iodophenyl group was estimated. **I(1)** forms an X-bond with the C═C π bond which provides 3.2 kcal/mol of stabilization. The total interaction energies based on the fragment that contains **I(2)** is −5.5 kcal/mol, while the fragment which contains **I(3)** has a slightly larger interaction energy of −6.4 kcal/mol. The directly calculated interaction energy of **CAT-3-perFPhI** and the substrate in **CAT-3-perFPhI-s-*trans*-1** is −15.5 kcal/mol.

For the purpose of comparison and also to gauge the predictive power of our calculations, the **Thiourea** catalyst employed by Hiersemann, Strassner and co-workers[34] is included (Scheme 1). Based on the TS provided by Hiersemann et al., we calculated the energetic span and TOF of the **Thiourea**-catalyzed Claisen rearrangement (see Scheme 1) at various temperatures. As evidenced in Table 6, the TOF for the **Thiourea**-catalyzed reaction at 318.15 K (or 45 °C) is 2 orders of magnitude higher than kK_{eq} of the uncatalyzed reaction. Given that the concentration of **Claisen-SM-1** is usually less than 1 M (0.05 M in the case of Hiersemann et al.), the results suggest that under saturation kinetic conditions (i.e., pseudo-zero-order with respect to reactant), a catalytic amount of **Thiourea** does not accelerate the Claisen rearrangement of **Claisen-SM-1** (TOF = rate/[**Thiourea**]$_{total}$. Therefore, in order for **Thiourea**-catalyzed Claisen rearrangement to be competitive, [**Thiourea**] has to be much more than 1 M). This is in qualitative agreement with the finding of Hiersemann et al.: a stoichiometric amount of **Thiourea** is required for an increase in the rate of Claisen rearrangement of **Claisen-SM-1**.[34]

For our designed XB-based catalyst **CAT-3-perFPhI**, the predicted TOF is at least an order of magnitude higher than that of the **Thiourea** catalyst (Table 6). With decreasing temperature, the difference between the kK_{eq} and TOF of **CAT-3-perFPhI** decreases, and at 273.15 K, the TOF becomes higher than the kK_{eq}, thus, allowing for the opportunity for catalytic Claisen rearrangement. Based on our result (see SI Table S2), chloroform is not a good choice of solvent. *n*-Hexane is predicted to be a better solvent for catalyzed Claisen rearrangement (Table 7). At 298.15 K, the TOF for **CAT-3-perFPhI** is an order of magnitude larger than the kK_{eq}. In addition, the TOF of **CAT-3-perFPhI** in *n*-hexane is at least an order of magnitude larger than the corresponding one in chloroform. In summary, XB catalysis based on **CAT-3-perFPhI** is applicable and feasible for Claisen rearrangement,

Table 7. Calculated Claisen Rearrangement Parameters in *n*-Hexane[a]

	uncatalyzed		**CAT-3-perFPhI**-catalyzed	
temp (K)	$\Delta G^{\ddagger}$ (kcal/mol)	$^{1}kK_{eq_1}$ (M h^{-1})	$\Delta G^{\ddagger}_{n\text{-hexane}}$ (kcal/mol)	TOF (h^{-1})
318.15	26.5	5.3×10^{-4}	28.3	8.6×10^{-4}
298.15	26.5	3.3×10^{-5}	27.3	2.3×10^{-4}
273.15	26.4	5.3×10^{-7}	26.0	2.5×10^{-5}

[a]Pre-equilibrium approximation rate constant under pseudo-zero-order condition.

DOI: 10.1021/acs.joc.6b01147
J. Org. Chem. 2016, 81, 7459−7470

but it requires a higher catalyst loading than the Diels–Alder reaction.

3.3. Cope-Type Hydroamination. Similar to Claisen rearrangement, Cope-type hydroamination has been demonstrated to be accelerated in protic solvent such as *i*Pr–OH[14,36] and catalyzed by hydrogen-bonding-based organocatalysts.[15] Based on our results on Diels–Alder and Claisen rearrangement, we envisaged that XB-based organocatalysts will be able to catalyze Cope-type hydroamination. Our model substrate with **CAT-3-perFPhI** is *N*-(pent-4-en-1-yl)hydroxylamine (Scheme 2), which is employed by Jacobsen and co-workers in their computational study on the feasibility of thiourea-catalyzed Cope-type hydroamination.[15]

Scheme 2. Model Cope-Type Hydroamination Reaction

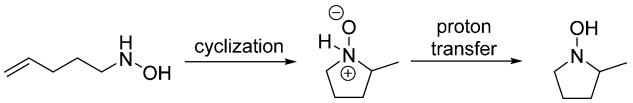

Table 8. Calculated Relative Energies[a] (kcal/mol) of Uncatalyzed Intramolecular Cope-Type Hydroamination Shown in Scheme 3

	Cope-Pre-TS	Cope-TS	Cope-P	Cope-TS2	Cope-P2
$\Delta H^{\ddagger}$ (gas phase)	0.00	19.9	1.3	28.0[b] (−7.6)[c]	−13.1
$\Delta H^{\ddagger}$ (*n*-hexane)	0.00	18.6	−1.8	23.2[b] (−8.0)[c]	−13.8
$\Delta G^{\ddagger}$ (gas phase)	1.8	24.2	4.9	31.4[b] (7.1)[c]	−9.9
$\Delta G^{\ddagger}$ (*n*-hexane)	1.8	22.9	1.8	26.7[b] (6.6)[c]	−10.6

[a]With respect to **Cope-R**. [b]Intramolecular proton transfer. [c]MeOH assisted proton transfer.

In the present study, we will assume that the proton transfer step is facile. Thus, we will focus only on the kinetic of the cyclization step (Scheme 2). This assumption is supported by the work of Beauchemin and co-workers[14] and our computational result; in the presence of a proton source such as alcohol, the barrier of proton transfer is lower than the cyclization step (Table 8). It should be noted that the intramolecular proton transfer has a higher barrier than the cyclization step (Scheme 3).

At the present level of theory, the uncatalyzed reaction has a barrier height of 24.2 kcal/mol in the gas phase (Table 8). A test for two common solvents: chloroform and *n*-hexane with single-point energy calculations indicate that $\Delta G^{\ddagger}$ will be lowered when these are employed as solvent (Table 8; see SI Table S4 for information on chloroform). Furthermore, our calculations predict that the uncatalyzed reaction proceeds with a similar $\Delta G^{\ddagger}$ value in chloroform and *n*-hexane for the cyclization step (please refer to SI for chloroform results).

The key stationary points of the potential energy surface calculated for **CAT-3-perFPhI**-catalyzed Cope-type hydroamination are summarized in Scheme 4. The corresponding change in Gibbs free energy in the gas phase, *n*-hexane, and chloroform relative to **Cope-R** and **CAT-3-perFPhI** are given in Table 9. The proton transfer from **Cope-PostTS-CAT** to **Cope-P2-CAT** (omitted in Scheme 4) assisted by MeOH is predicted to have a small barrier ($\Delta G^{\ddagger}$) of 1.1 kcal/mol in *n*-hexane solvent.

Our calculations indicate that only $\Delta G^{\ddagger}$ in the gas phase for **CAT-3-perFPhI** catalyzed Cope-type hydroamination is lower than the uncatalyzed one (Table 9). The inclusion of solvation effect via SMD solvation model virtually removes the reduction in $\Delta G^{\ddagger}$ due to noncovalent interaction between **CAT-3-perFPhI** and the substrate in the TS (Table 9). In chloroform solvent, the complex between **CAT-3-perFPhI** and product (**Cope-P2**) is more stable than the free product and catalyst (Table 9, compared with the energetic span of 24.7 kcal/mol). This results in product inhibition and an increase in the energetic span (TDI is **Cope-P2-CAT**). However, in *n*-hexane which is the solvent employed experimentally by the group of Jacobsen, **Cope-P2-CAT** is higher in free energy than the free product and catalyst, and therefore, the TDI becomes the free

Scheme 3. Reaction Pathway for Uncatalyzed Intramolecular Cope-Type Hydroamination

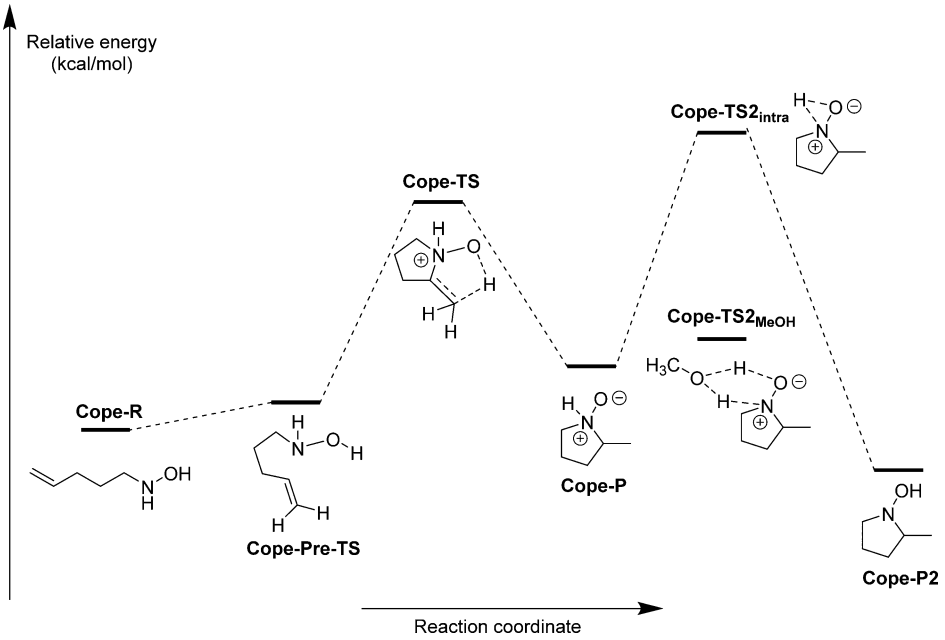

DOI: 10.1021/acs.joc.6b01147
J. Org. Chem. 2016, 81, 7459–7470

Scheme 4. Schematic Reaction Profile of CAT-3-perFPhI-Catalyzed Cope-Type Hydroamination

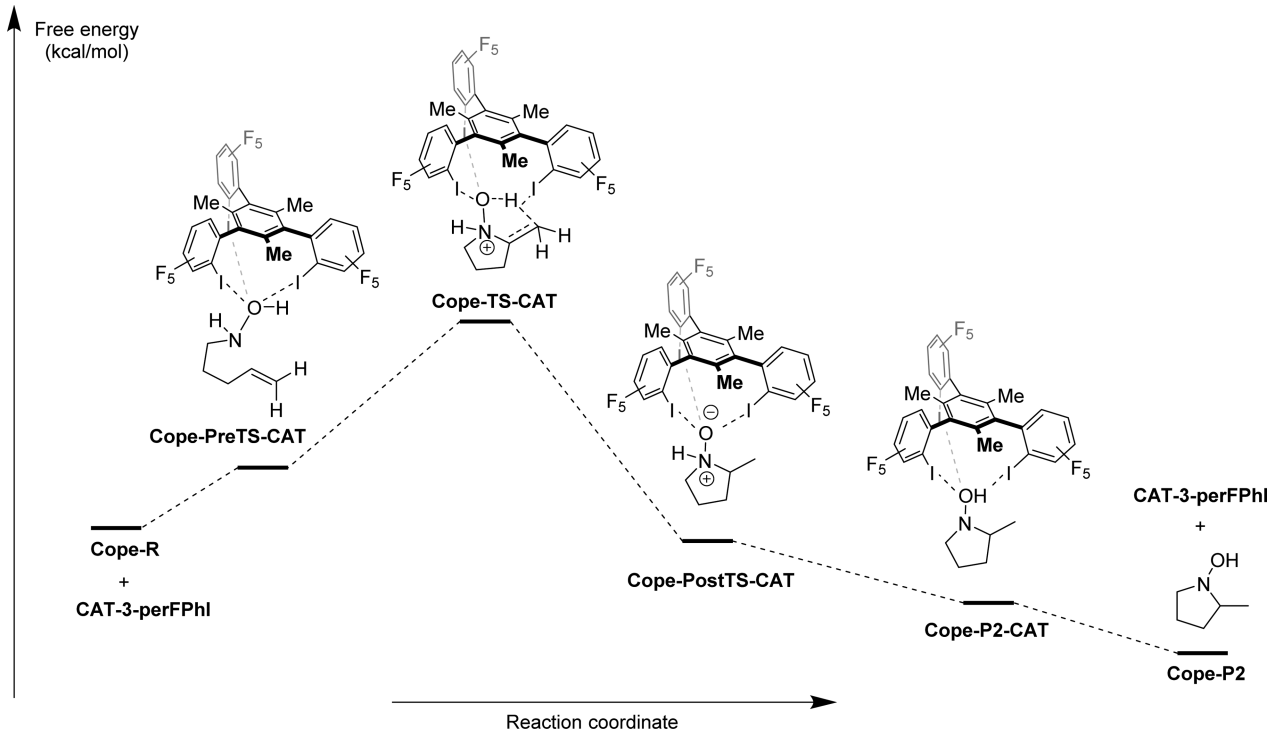

Table 9. Calculated Relative Free Energies[a] (kcal/mol) for Scheme 4

species	ΔG (gas)	ΔG (*n*-hexane)	ΔG (chloroform)
Cope-Pre-TS-CAT	3.6	5.0	6.2
Cope-TS-CAT	22.2 (24.2)[b]	22.9 (22.9)[b]	24.2 (22.9)[b]
Cope-PostTS-CAT	−7.6	−8.1	−7.8
Cope-P2-CAT	−11.8	−15.2	−15.6
Cope-P2 + CAT-3-perFPhI	−15.6	−17.9	−15.1

[a]With respect to **Cope-R** + **CAT-3-perFPhI**. [b]Uncatalyzed results in parentheses.

reactant and catalyst. The energetic span becomes equal to the barrier as defined by the difference between **Cope-TS-CAT** and **Cope-R** + **CAT-3-perFPhI**.

Temperature and TOF. In contrast to the trend in TOF for the Diels−Alder reaction, the maximum TOF is at 273.15 K (Table 10). Further lowering of temperature does not result in a significant increase in TOF. At 273.15 K, the TOF of the **CAT-3-perFPhI** catalyzed Cope-type hydroamination is approximately 30 times larger than the kK_{eq} of the uncatalyzed reaction. At 248.15 K, this difference becomes 281 times larger,

Table 10. Calculated Parameters of CAT-3-perFPhI-Cope-Type Hydroamination in *n*-Hexane

	$\Delta G^{\ddagger}_{n\text{-hexane}}$ (kcal/mol)		uncatalyzed	**CAT-3-perFPhI**
Temp	uncatalyzed	**CAT-3-perFPhI**	kK_{eq}[a]/ $M\ h^{-1}$	TOF_{3B}/h^{-1}
298.15 K	22.9	22.9	0.3	0.4
273.15 K	21.8	20.1	0.06	1.8
248.15 K	21.6	18.8	0.002	0.5

[a]Pre-equilibrium approximation rate constant under pseudo-zero-order condition.

thus allowing for a catalytic amount of **CAT-3-perFPh** to be used.

Analysis of Noncovalent Interaction in Cope-Type Hydroamination TS. Analysis of intermolecular interactions with the NCI plot reveals that in addition to two strong X-bonds between iodines [**I(1)** and **I(2)** in Figure 9] of **CAT-3-perFPhI** and the oxygen of the substrate, a third X-bond between iodine **I(3)** of **CAT-3-perFPhI** and the C−H σ bond is present. The interaction energy between the catalyst and substrate in **cope-TS-CAT** is −14.3 kcal/mol. The interaction energy of the fragment which contains **I(2)** is −5.8 kcal/mol. It is lower than that of the fragment which contains **I(1)** by 0.5 kcal/mol due to the presence of weak hydrogen bonds between the lone pair of **I(1)** and the C−H bonds of the substrate (Figure 9; refer to Figure S4 and SI for further discussion[39]). Interestingly, there is a halogen bond between iodine **I(3)** of **CAT-3-perFPhI** and the σ bond of C−H. This is somewhat analogous to the X-bond between the C=C or C=O π bond and a halogen which is observed in both the Diels−Alder and Claisen rearrangement reported in preceding sections. However, to the best of our knowledge, such an X-bond between a developing σ bond and halogen in the TS has not been documented in the literature.

To provide a semiqualitative estimate of the strength of such a halogen bond, we modified **CAT-3-perFPhI** and calculated the effect of substitution on atom(s) that is (are) involved in the σ-iodine X-bond on the cyclization barriers (Table 11). The reaction barriers $\Delta E^{\ddagger}$ provide information on the strength of the σ-iodine X-bond. By replacing the affected I with F (i.e., from **CAT-3-perFPhI** to **CAT-3-perF**), the X-bond strength weakens from I to F, with a corresponding increase of 2.6 kcal/mol in $\Delta E^{\ddagger}$. Similarly, by changing the perfluoroiodophenyl group to the phenyl group, we expect that the stabilizing σ-iodine XB interaction will disappear. Indeed, our calculation corroborates this: an increase of 2.6 kcal/mol in $\Delta E^{\ddagger}$ (i.e., **CAT-3-perFPhI** to **CAT-2-perF-1-PhH**). Ongoing from

DOI: 10.1021/acs.joc.6b01147
J. Org. Chem. 2016, 81, 7459−7470

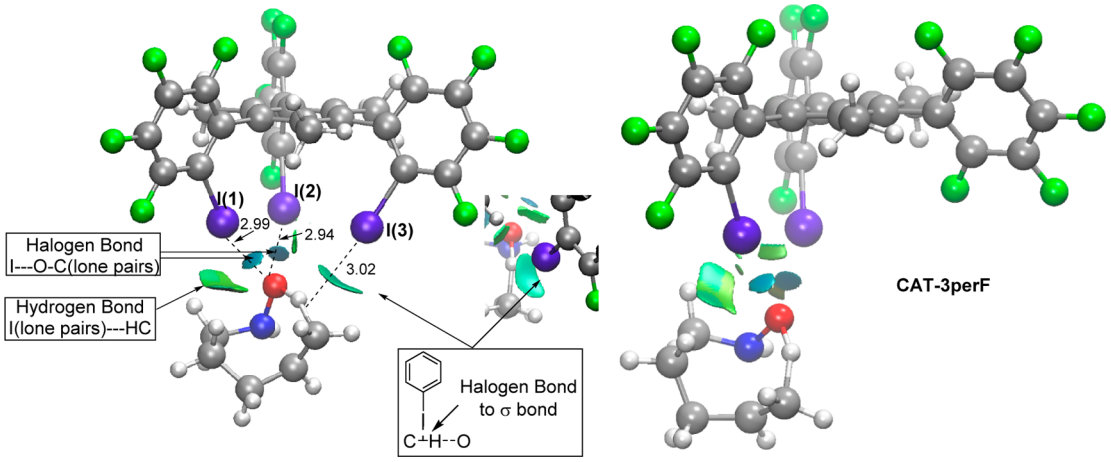

Figure 9. NCI isosurfaces for key intermolecular interactions found in the transition states of **CAT-3-perFPhI**- and **CAT-3perF**-Cope-type hydroamination. **I(1)–I(3)** are halogen bond distances in Å.

Table 11. Effect of Substitution/Removal of Halogen Involved in the σ-Type Halogen Bond on the Activation Barrier (in kcal/mol) of Catalyzed Cope-Type Hydroamination

	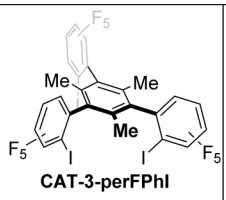 CAT-3-perFPhI	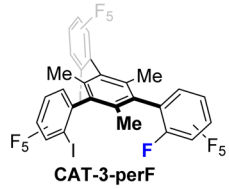 CAT-3-perF	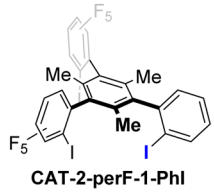 CAT-2-perF-1-PhI	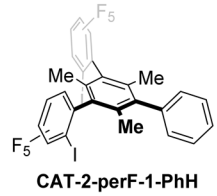 CAT-2-perF-1-PhH
$\Delta E^{\neq}$	7.8	10.3	8.9	10.3
$\Delta H^{\neq}$	6.7	8.5	7.0	8.6
$\Delta G^{\neq}$	22.2	23.3	23.3	24.5

Table 12. Calcuated Gas-Phase Relative Free Energies (in kcal/mol) and TOFs of Uncatalyzed and Catalyzed Diels–Alder Reactions[a]

	uncatalyzed reaction[b]			**CAT-perF**-catalyzed reaction	
method	$\Delta G_{\text{pre-TS}}$	$\Delta G^{\ddagger}$	$\Delta G^{\ddagger} + \Delta G_{\text{pre-TS}}$	energetic span	TOF
M06-2X	4.2	17.3	21.6	19.3	0.18
M06-2X-D3	3.8	17.4	21.2	18.9	0.42
M11	4.4	17.5	21.9	19.7	9.2×10^{-2}
ω-B97X-D	5.0	19.3	24.3	22.0	5.0×10^{-4}
B3LYP-D3	5.7	17.8	23.5	21.3	3.4×10^{-3}
PBE0	9.8	13.2	23.0	26.3	1.4×10^{-7}
PBE0-D3	5.4	12.9	18.3	16.0	151
B97-D3	4.8	12.9	17.7	15.3	580
MP2	4.2	8.3	12.5		
CCSD(T)	6.0	17.0	22.9		
CCSD(T)-F12[c]	5.4	16.7	22.1		

[a]Based on geometry optimization and frequency calculation at M06-2X/6-31G(d) level. Basis set for single-point energy calculations is 6-311+G(d,p). Temperature = 248.15 K. [b]For definition of $\Delta G^{\ddagger} + \Delta G_{\text{pre-TS}}$, refer to Figure 3. [c]aug-cc-pVDZ basis set.

perfluoroiodophenyl to iodophenyl (i.e., from **CAT-3-perFPhI** to **CAT-2-perF-1PhI**), which is expected to weaken the σ-iodine X-bond, an increase of $\Delta E^{\ddagger}$ by 1.2 kcal/mol resulted. Based on these results, we estimated the σ-iodine X-bond to be worth ∼2.6 kcal/mol of stabilization. For comparison, the interaction energy of this σ-iodine X-bond estimated by the fragment approach outlined in Figure 6 is −2.8 kcal/mol.

Comparing the optimized geometries of the transition states for **CAT-3-perFPhI** and **CAT-3-perF** (Figure 9) indicates that the substrate tilted to one side in the absence of the third perfluoroiodophenyl group. This structural difference readily reflects the presence of a stabilizing interaction, which is further supported by NCI analysis (Figure 9).

DOI: 10.1021/acs.joc.6b01147
J. Org. Chem. 2016, 81, 7459–7470

3.4. Benchmarking of DFT Methods for Halogen Bond Catalysis.

Due to the long interaction distance of the halogen bond activation (3.0−3.5 Å) and the presence of other noncovalent interactions (e.g., C−H···I) in the key transition states, proper treatment of long-range dispersion in the DFT method employed is expected to be important. Based on extensive benchmark studies of geometries and dissociation energies of halogen bonded complexes, the M06-2X functional has shown to be sufficiently reliable.[18] However, similar performance assessment on transition states involving halogen bond is lacking. Thus, we have examined the performance of several popular DFT methods and the dispersion corrected counterparts on the reaction barriers for both uncatalyzed and catalyzed (i.e., energetic span) Diels−Alder reaction (Table 12). In these benchmark calculations, single-point calculations using the 6-311+G(d,p) basis set was employed, based on the M06-2X/6-31G* optimized geometries. Our best theoretical estimates correspond to the results obtained at the CCSD(T)-F12/aug-cc-pVDZ level. The CCSD(T)-F12 method is known to offer a gain in 2−3 ζ steps in accuracy of the CCSD(T) result based on the size of the basis set; thus, it allows the electronic energy of CCSD(T)-F12/aug-cc-pVDZ to reach the accuracy of aug-cc-pVTZ or aug-cc-pVQZ.[37]

As evidenced in Table 12, various DFT functionals give a range of results for both the catalyzed and uncatalyzed Diels−Alder reactions. For the uncatalyzed reaction, M06-2X and M11 yield results that are closest to the CCSD(T) reference, i.e. CCSD(T)-F12/aug-cc-pVDZ level. Unfortunately, CCSD(T)-F12/aug-cc-pVDZ calculations for the catalyzed reaction is not within our reach computationally. Nevertheless, it can be assumed that M06-2X give reasonable results based on the additional benchmark results of Claisen rearrangement and Cope-Type hydroamination (see Tables S7−S10 in SI). The importance of dispersion correction in the DFT functional is evident from the comparison of the results for PBE0 and PBE-D3 (Table 12). As M06-2X, which is employed in this computational study, has already accounted for dispersion through the training of its functional parameters with a training set that contains dispersion information, the inclusion of D3 correction (i.e., M06-2X-D3) does not make a significant impact to the results. It is worth noting that, with the 6-311+G(d,p) basis set, MP2 severely underestimates the barrier compared to the CCSD(T) reference.

We have explored also the effect of the basis set on geometry optimization and frequency calculation. For the Diels−Alder reaction considered here, the use of a larger 6-311G(d) basis set has minimal impact on our computational results (see SI Table S5). In particular, it does not change our conclusion when we compared the reaction barrier and energetic span. Finally, we examined the effect of hindered rotor correction. The overestimation of the partition function when the hindered rotor is approximated as a harmonic oscillator is well established. This could potentially lead to a large error in calculated barrier. Here, we applied 1D hindered rotor correction[38,39] to the uncatalyzed and catalyzed Diels−Alder reactions and found insignificant change in the calculated barrier and energy span (see SI Table S6). This is due mainly to the cancellation of error. In summary, various benchmark calculations lend us confidence in the M06-2X predicted reaction barriers and turnover frequencies in halogen bond catalysis.

4. CONCLUSION

In conclusion, we have demonstrated, within the limits of the theoretical methods employed, the feasibility of halogen bonding catalysis in Diels−Alder reaction, Claisen rearrangement, and Cope-type hydroamination. Our designed tripodal organocatalyst have three halogen bond donors, namely perfluoro-iodophenyl groups. The iodine atoms are able to provide strong stabilization in terms of halogen bond and secondary interaction via its lone pair. In all three reactions, multiple halogen bonds, involving a lone pair, π bond, and even σ bond as halogen bond acceptors, are observed in the key transition states. The cooperative noncovalent interactions are sufficiently strong (~15 kcal/mol) to drive the molecular recognition in various transition states. A novel X-bond between the C−H σ bond and iodine is disclosed. We acknowledged that the translation of computational results remains a challenging issue.[40] For instance, we have considered the reaction pathway to form the desired product, but not deactivating pathways such as stability of the catalyst and undiscovered competing pathways. Nevertheless, we hope this computational work will further stimulate experimental work in halogen bonding catalysis.

■ ASSOCIATED CONTENT

Supporting Information

The Supporting Information is available free of charge on the ACS Publications website at DOI: 10.1021/acs.joc.6b01147.

Additional computational results, total energies (PDF)

Cartesian coordinates of all optimized structures (ZIP)

■ AUTHOR INFORMATION

Corresponding Author

*E-mail: chmwmw@nus.edu.sg.

Notes

The authors declare no competing financial interest.

■ ACKNOWLEDGMENTS

This research was supported by the National University of Singapore (Grant No: R-143-000-555-112).

■ REFERENCES

(1) Desiraju, G. R.; Ho, P. S.; Kloo, L.; Legon, A. C.; Marquardt, R.; Metrangolo, P.; Politzer, P.; Resnati, G.; Rissanen, K. *Pure Appl. Chem.* **2013**, *85*, 1711−1713.

(2) (a) Corradi, E.; Meille, S. V.; Messina, M. T.; Metrangolo, P.; Resnati, G. *Angew. Chem., Int. Ed.* **2000**, *39*, 1782−1786. (b) Metrangolo, P.; Resnati, G. *Chem. - Eur. J.* **2001**, *7*, 2511−2519. (c) Aakeröy, C. B.; Fasulo, M.; Schultheiss, N.; Desper, J.; Moore, C. *J. Am. Chem. Soc.* **2007**, *129*, 13772−13773. (d) Metrangolo, P.; Meyer, F.; Pilati, T.; Resnati, G.; Terraneo, G. *Angew. Chem., Int. Ed.* **2008**, *47*, 6114−6127. (e) Vargas Jentzsch, A.; Emery, D.; Mareda, J.; Metrangolo, P.; Resnati, G.; Matile, S. *Angew. Chem., Int. Ed.* **2011**, *50*, 11675−11678. (f) Priimagi, A.; Cavallo, G.; Metrangolo, P.; Resnati, G. *Acc. Chem. Res.* **2013**, *46*, 2686−2695.

(3) (a) Auffinger, P.; Hays, F. A.; Westhof, E.; Ho, P. S. *Proc. Natl. Acad. Sci. U. S. A.* **2004**, *101*, 16789−16794. (b) Scholfield, M. R.; Vander Zanden, C. M.; Carter, M.; Ho, P. S. *Protein Sci.* **2013**, *22*, 139−152.

(4) (a) Bruckmann, A.; Pena, M. A.; Bolm, C. *Synlett* **2008**, *2008*, 900−902. (b) Kniep, F.; Jungbauer, S. H.; Zhang, Q.; Walter, S. M.; Schindler, S.; Schnapperelle, I.; Herdtweck, E.; Huber, S. M. *Angew. Chem., Int. Ed.* **2013**, *52*, 7028−7032. (c) He, W.; Ge, Y.-C.; Tan, C.-H. *Org. Lett.* **2014**, *16*, 3244−3247. (d) Jungbauer, S. H.; Walter, S.

DOI: 10.1021/acs.joc.6b01147
J. Org. Chem. 2016, 81, 7459−7470

M.; Schindler, S.; Rout, L.; Kniep, F.; Huber, S. M. *Chem. Commun.* **2014**, *50*, 6281−6284. (e) Jungbauer, S. H.; Huber, S. M. *J. Am. Chem. Soc.* **2015**, *137*, 12110−12120. (f) Takeda, Y.; Hisakuni, D.; Lin, C.-H.; Minakata, S. *Org. Lett.* **2015**, *17*, 318−321. (g) Heinz, N.; Dolg, M.; Albrecht Berkessel, A. *J. Comput. Chem.* **2015**, *36*, 1812−1817. (h) Nziko, V. d. P. N.; Scheiner, S. *J. Org. Chem.* **2016**, *81*, 2589.

(5) Jungbauer, S. H.; Schindler, S.; Kniep, F.; Walter, S. M.; Rout, L.; Huber, S. M. *Synlett* **2013**, *24*, 2624−2628.

(6) Zong, L.; Ban, X.; Kee, C. W.; Tan, C.-H. *Angew. Chem., Int. Ed.* **2014**, *53*, 11849−11853.

(7) Metrangolo, P.; Neukirch, H.; Pilati, T.; Resnati, G. *Acc. Chem. Res.* **2005**, *38*, 386−395.

(8) (a) Schreiner, P. R. *Chem. Soc. Rev.* **2003**, *32*, 289−296. (b) Taylor, M. S.; Jacobsen, E. N. *Angew. Chem., Int. Ed.* **2006**, *45*, 1520−1543. (c) Doyle, A. G.; Jacobsen, E. N. *Chem. Rev.* **2007**, *107*, 5713−5743. (d) Marcelli, T. *Ideas in Chemistry and Molecular Sciences*; Wiley-VCH Verlag GmbH & Co. KGaA: 2010. (e) Johnston, R. C.; Cheong, P. H.-Y. *Org. Biomol. Chem.* **2013**, *11*, 5057−5064.

(9) Beletskiy, E. V.; Schmidt, J.; Wang, X.-B.; Kass, S. R. *J. Am. Chem. Soc.* **2012**, *134*, 18534−18537.

(10) Linke, A.; Jungbauer, S. H.; Huber, S. M.; Waldvogel, S. R. *Chem. Commun.* **2015**, *51*, 2040−2043.

(11) Severance, D. L.; Jorgensen, W. L. *J. Am. Chem. Soc.* **1992**, *114*, 10966−10968.

(12) (a) Beale, T. M.; Chudzinski, M. G.; Sarwar, M. G.; Taylor, M. S. *Chem. Soc. Rev.* **2013**, *42*, 1667−1680. (b) Cavallo, G.; Metrangolo, P.; Pilati, T.; Resnati, G.; Sansotera, M.; Terraneo, G. *Chem. Soc. Rev.* **2010**, *39*, 3772−3783. (c) Vargas Jentzsch, A.; Hennig, A.; Mareda, J.; Matile, S. *Acc. Chem. Res.* **2013**, *46*, 2791−2800.

(13) (a) House, H. O.; Manning, D. T.; Melillo, D. G.; Lee, L. F.; Haynes, O. R.; Wilkes, B. E. *J. Org. Chem.* **1976**, *41*, 855−863. (b) House, H. O.; Lee, L. F. *J. Org. Chem.* **1976**, *41*, 863−869. (c) Oppolzer, W.; Spivey, A. C.; Bochet, C. G. *J. Am. Chem. Soc.* **1994**, *116*, 3139−3140. (d) Cooper, N. J.; Knight, D. W. *Tetrahedron* **2004**, *60*, 243−269.

(14) Beauchemin, A. M.; Moran, J.; Lebrun, M.-E.; Séguin, C.; Dimitrijevic, E.; Zhang, L.; Gorelsky, S. I. *Angew. Chem., Int. Ed.* **2008**, *47*, 1410−1413.

(15) Brown, A. R.; Uyeda, C.; Brotherton, C. A.; Jacobsen, E. N. *J. Am. Chem. Soc.* **2013**, *135*, 6747−6749.

(16) (a) Zhao, Y.; Truhlar, D. G. *Acc. Chem. Res.* **2008**, *41*, 157−167. (b) Zhao, Y.; Truhlar, D. *Theor. Chem. Acc.* **2008**, *120*, 215−241.

(17) (a) Rokob, T. A.; Hamza, A.; Papai, I. *Org. Lett.* **2007**, *9*, 4279−4282. (b) Yang, H.; Wong, M. W. *J. Am. Chem. Soc.* **2013**, *135*, 5808−5818. (c) Cho, B.; Tan, C.-H.; Wong, M. W. *J. Org. Chem.* **2012**, *77*, 6553−6562. (d) Wong, M. W.; Ng, E. A. M. *Aust. J. Chem.* **2014**, *67*, 1100−1109.

(18) (a) Kozuch, S.; Martin, J. M. L. *J. Chem. Theory Comput.* **2013**, *9*, 1918−1931. (b) Doemer, M.; Tavernelli, I.; Rothlisberger, U. *J. Chem. Theory Comput.* **2013**, *9*, 955−964. (c) Forni, A.; Pieraccini, S.; Rendine, S.; Sironi, M. *J. Comput. Chem.* **2014**, *35*, 386−394. (d) Zhang, U.; Ma, N.; Wang, W. *J. Theor. Comput. Chem.* **2012**, *11*, 1165−1173.

(19) Martin, J. M. L.; Sundermann, A. *J. Chem. Phys.* **2001**, *114*, 3408−3420.

(20) (a) Feller, D. *J. Comput. Chem.* **1996**, *17*, 1571−1586. (b) Schuchardt, K. L.; Didier, B. T.; Elsethagen, T.; Sun, L.; Gurumoorthi, V.; Chase, J.; Li, J.; Windus, T. L. *J. Chem. Inf. Model.* **2007**, *47*, 1045−1052.

(21) Marenich, A. V.; Cramer, C. J.; Truhlar, D. G. *J. Phys. Chem. B* **2009**, *113*, 6378−6396.

(22) Frisch, M. J.; Trucks, G. W.; Schlegel, H. B.; Scuseria, G. E.; Robb, M. A.; Cheeseman, J. R.; Scalmani, G.; Barone, V.; Mennucci, B.; Petersson, G. A.; Nakatsuji, H.; Caricato, M.; Li, X.; Hratchian, H. P.; Izmaylov, A. F.; Bloino, J.; Zheng, G.; Sonnenberg, J. L.; Hada, M.; Ehara, M.; Toyota, K.; Fukuda, R.; Hasegawa, J.; Ishida, M.; Nakajima, T.; Honda, Y.; Kitao, O.; Nakai, H.; Vreven, T.; Montgomery, J. A.; Peralta, J. E.; Ogliaro, F.; Bearpark, M.; Heyd, J. J.; Brothers, E.; Kudin, K. N.; Staroverov, V. N.; Kobayashi, R.; Normand, J.; Raghavachari, K.; Rendell, A.; Burant, J. C.; Iyengar, S. S.; Tomasi, J.; Cossi, M.; Rega, N.; Millam, J. M.; Klene, M.; Knox, J. E.; Cross, J. B.; Bakken, V.; Adamo, C.; Jaramillo, J.; Gomperts, R.; Stratmann, R. E.; Yazyev, O.; Austin, A. J.; Cammi, R.; Pomelli, C.; Ochterski, J. W.; Martin, R. L.; Morokuma, K.; Zakrzewski, V. G.; Voth, G. A.; Salvador, P.; Dannenberg, J. J.; Dapprich, S.; Daniels, A. D.; Farkas; Foresman, J. B.; Ortiz, J. V.; Cioslowski, J.; Fox, D. J. *Gaussian 09*, revision D.01; Wallingford, CT, 2009.

(23) Adler, T. B.; Knizia, G.; Werner, H.-J. *J. Chem. Phys.* **2007**, *127*, 221106−221109.

(24) Werner, H.-J.; Knowles, P. J.; Knizia, G.; Manby, F. R.; Schütz, M.; Celani, P.; Györffy, W.; Kats, D.; Korona, T.; Lindh, R.; Mitrushenkov, A.; Rauhut, G.; Shamasundar, K. R.; Adler, T. B.; Amos, R. D.; Bernhardsson, A.; Berning, A.; Cooper, D. L.; Deegan, M. J. O.; Dobbyn, A. J.; Eckert, F.; Goll, E.; Hampel, C.; Hesselmann, A.; Hetzer, G.; Hrenar, T.; Jansen, G.; Köppl, C.; Liu, Y.; Lloyd, A. W.; Mata, R. A.; May, A. J.; McNicholas, S. J.; Meyer, W.; Mura, M. E.; Nicklaß, A.; O'Neill, D. P.; Palmieri, P.; Peng, D.; Pflüger, K.; Pitzer, R.; Reiher, M.; Shiozaki, T.; Stoll, H.; Stone, A. J.; Tarroni, R.; Thorsteinsson, T.; Wang, M. *MOLPRO*, Version 2015.1; see http://www.molpro.net.

(25) Johnson, E. R.; Keinan, S.; Mori-Sánchez, P.; Contreras-García, J.; Cohen, A. J.; Yang, W. *J. Am. Chem. Soc.* **2010**, *132*, 6498−6506.

(26) Contreras-García, J.; Johnson, E. R.; Keinan, S.; Chaudret, R.; Piquemal, J.-P.; Beratan, D. N.; Yang, W. *J. Chem. Theory Comput.* **2011**, *7*, 625−632.

(27) Humphrey, W.; Dalke, A.; Schulten, K. *J. Mol. Graphics* **1996**, *14*, 33−38.

(28) Legault, C. Y. 1.0.562 BETA ed.; Université de Sherbrooke: 2012.

(29) Zhou, Q.; Li, Y. *J. Am. Chem. Soc.* **2015**, *137*, 10182−10189.

(30) (a) Kozuch, S.; Shaik, S. *Acc. Chem. Res.* **2011**, *44*, 101−110. (b) Liu, P.; Cheong, P. H.-Y.; Yu, Z.-X.; Wender, P. A.; Houk, K. N. *Angew. Chem., Int. Ed.* **2008**, *47*, 3939. (c) Xu, X.; Liu, P.; Lesser, A.; Sirois, L. E.; Wender, P. A.; Houk, K. N. *J. Am. Chem. Soc.* **2012**, *134*, 11012. (d) Mustard, T. J. L.; Wender, P. A.; Cheong, P. H.-Y. *ACS Catal.* **2015**, *5*, 1758.

(31) (a) Politzer, P.; Lane, P.; Concha, M.; Ma, Y.; Murray, J. *J. Mol. Model.* **2007**, *13*, 305−311. (b) Bundhun, A.; Ramasami, P.; Murray, J.; Politzer, P. *J. Mol. Model.* **2013**, *19*, 2739−2746.

(32) (a) Kozuch, S.; Shaik, S. *J. Am. Chem. Soc.* **2006**, *128*, 3355−3365. (b) Uhe, A.; Kozuch, S.; Shaik, S. *J. Comput. Chem.* **2011**, *32*, 978−985.

(33) (a) Martín Castro, A. M. *Chem. Rev.* **2004**, *104*, 2939−3002. (b) Majumdar, K. C.; Nandi, R. K. *Tetrahedron* **2013**, *69*, 6921−6957.

(34) Kirsten, M.; Rehbein, J.; Hiersemann, M.; Strassner, T. *J. Org. Chem.* **2007**, *72*, 4001−4011.

(35) (a) Uyeda, C.; Jacobsen, E. N. *J. Am. Chem. Soc.* **2008**, *130*, 9228−9229. (b) Uyeda, C.; Rötheli, A. R.; Jacobsen, E. N. *Angew. Chem., Int. Ed.* **2010**, *49*, 9753−9756. (c) Uyeda, C.; Jacobsen, E. N. *J. Am. Chem. Soc.* **2011**, *133*, 5062−5075.

(36) Moran, J.; Gorelsky, S. I.; Dimitrijevic, E.; Lebrun, M.-E.; Bédard, A.-C.; Séguin, C.; Beauchemin, A. M. *J. Am. Chem. Soc.* **2008**, *130*, 17893−17906.

(37) (a) Knizia, G.; Adler, T. B.; Werner, H.-J. *J. Chem. Phys.* **2009**, *130*, 54104−54124. (b) Kong, L.; Bischoff, F. A.; Valeev, E. F. *Chem. Rev.* **2012**, *112*, 75−107.

(38) (a) Truhlar, D. G. *J. Comput. Chem.* **1991**, *12*, 266. (b) Ayala, P. Y.; Schlegel, H. B. *J. Chem. Phys.* **1998**, *108* (6), 2314.

(39) Lu, T.; Chen, F. *J. Comput. Chem.* **2012**, *33* (5), 580.

(40) Hoffmann, R.; Schleyer, P. v. R.; Schaefer, H. *Angew. Chem., Int. Ed.* **2008**, *47*, 7164.

DOI: 10.1021/acs.joc.6b01147
J. Org. Chem. 2016, 81, 7459−7470